Electronic Supplementary Material (ESI) for Journal of Materials Chemistry A.

Supporting information

Formation of porous MoO_2@C nano-octahedrons from a polyoxometalate-based metal-organic framework for highly reversible lithium storage

Guoliang Xia[1], Dong Liu[1], Fangcai Zheng[1], Yang Yang[1], Jianwei Su[1], Qianwang Chen[1,2]

1 Hefei National Laboratory for Physical Science at Microscale, Department of Materials Science & Engineering & Collaborative Innovation Center of Suzhou Nano Science and Technology, University of Science and Technology of China, Hefei 230026, China.

2 High Magnetic Field Laboratory, Hefei Institutes of Physical Science, Chinese Academy of Sciences, Hefei 230031, China. Correspondence and requests for materials should be addressed to Q.C. (email: cqw@ustc.edu.cn).

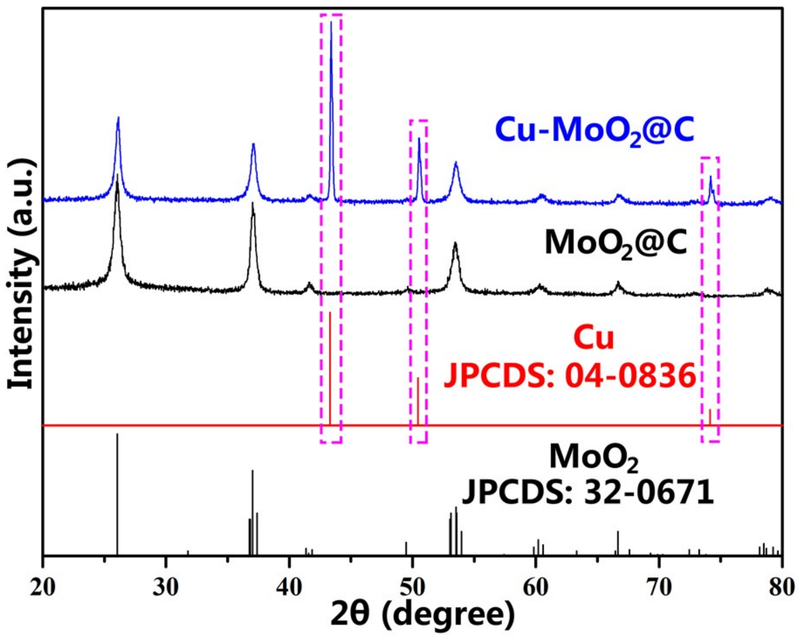

Figure S1. XRD patterns of Cu-MoO_2@C and MoO_2@C. This pattern clearly indicates that the metallic Cu could be completely removed after the treatment with the aqueous solution of $FeCl_3$.

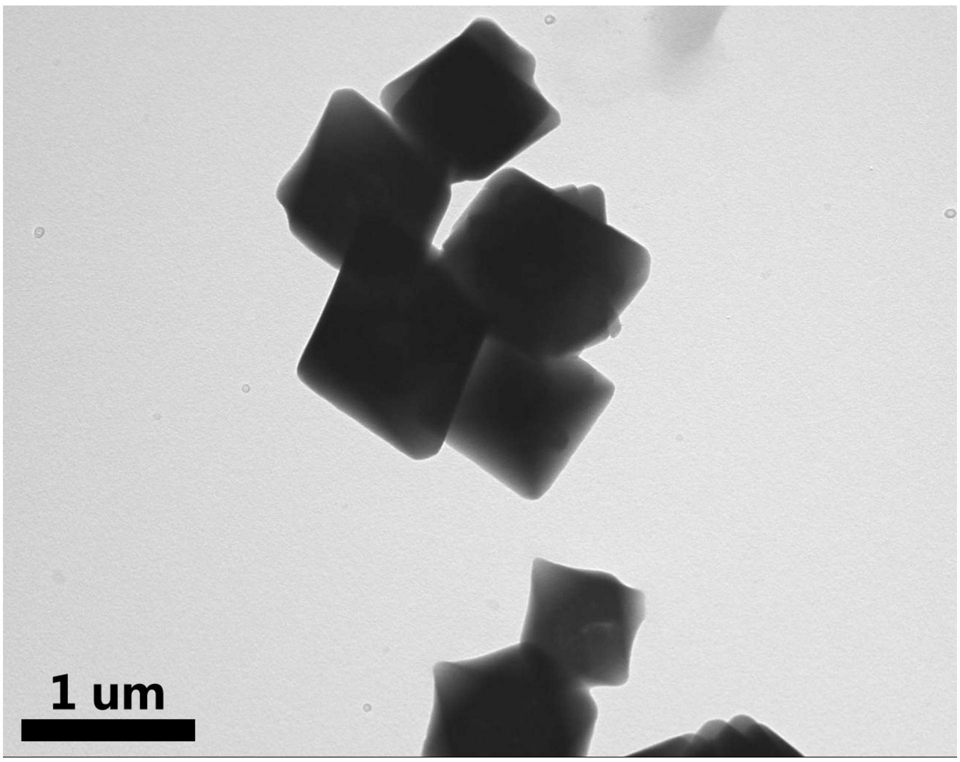

Figure S2. TEM image of NENU-5.

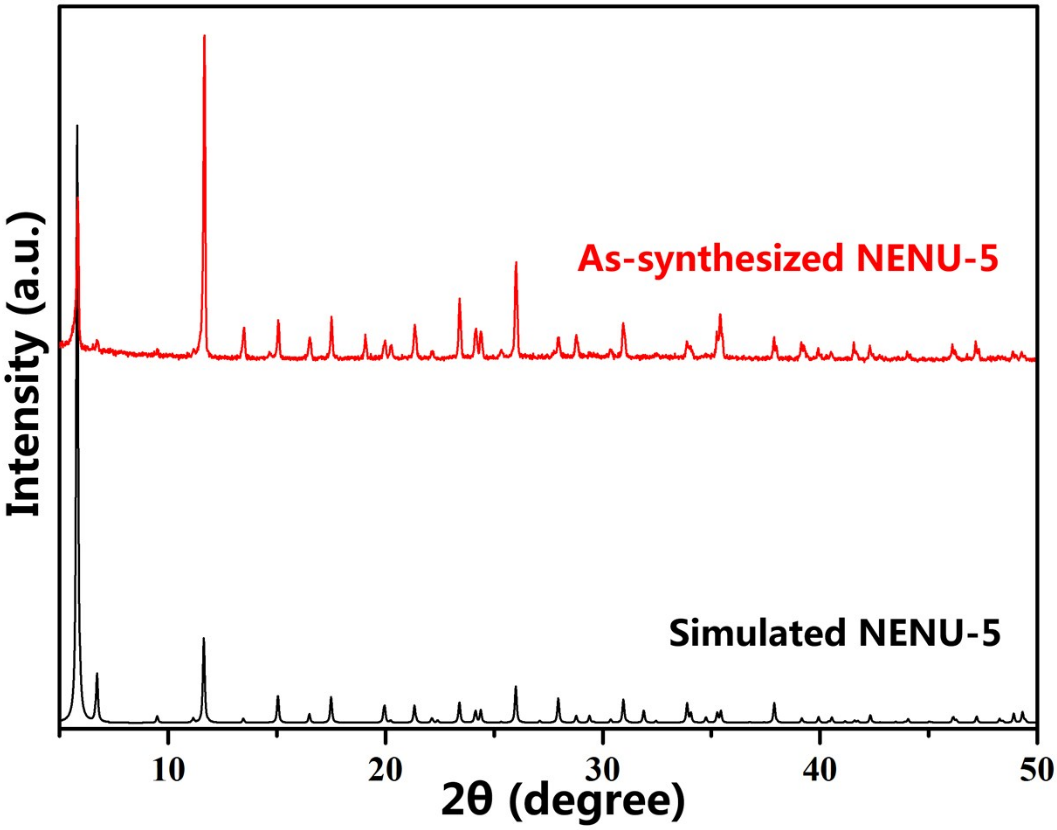

Figure S3. XRD patterns of as-synthesized NENU-5 and simulated NENU-5.

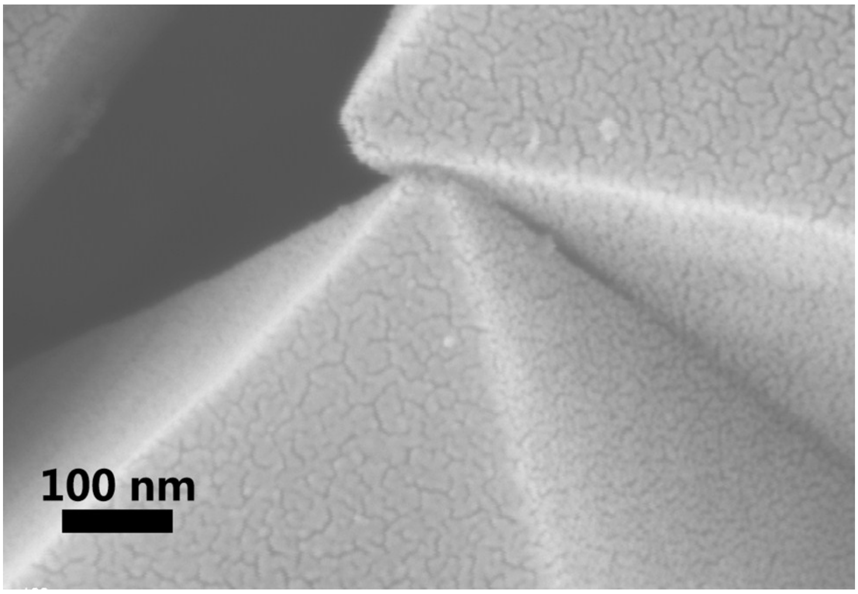

Figure S4. FESEM of as-prepared MoO2@C nano-octahedron.

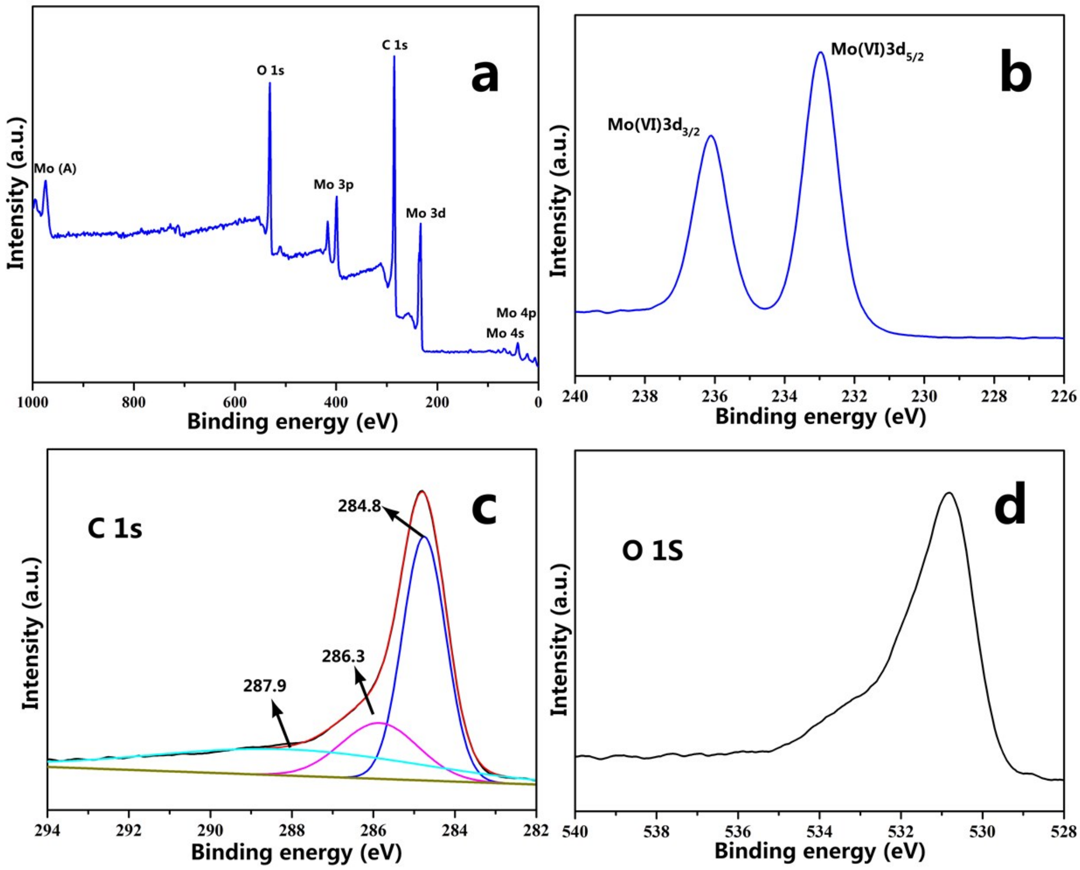

Figure S5. XPS spectra of (a) MoO_2@C, (b) Mo 3d, (c) C 1s, (d) O1s.

As displayed in Figure S5b,respectively, two pronounced main peaks are located at 232.9 eV and 236.1 eV , which could be resigned to Mo $3d_{5/2}$ and Mo $3d_{3/2}$ binding energy of Mo(Ⅵ) oxidation state. There are none peaks related to Mo(Ⅳ) $3d_{5/2}$ or Mo(Ⅳ) $3d_{3/2}$, which are the main composition according to the result of the power X-Ray diffraction (XRD). The reasons can be as follows. Firstly, XPS only distinguish the valence state and composition of the sample's surface, while the composition of bulk phase is what XRD characterizes; on the other hand, deriving from surface oxidation of metastable of MoO_2 when exposed to air, Mo(Ⅵ) is discovered, which can also mean that the majority of MoO_2 are coated by carbon matrix. The high-resolution C1s spectrum is displayed in Figure S5c, the main peak at 284.8 eV indicates that the graphite carbon is the majority. The C-O and C=O bonds at 286.3 eV and 287.9 eV, respectively, are also shown in C1s spectrum. The O1s peaks are broad suggesting the different chemical states of oxygen (Figure S5d).

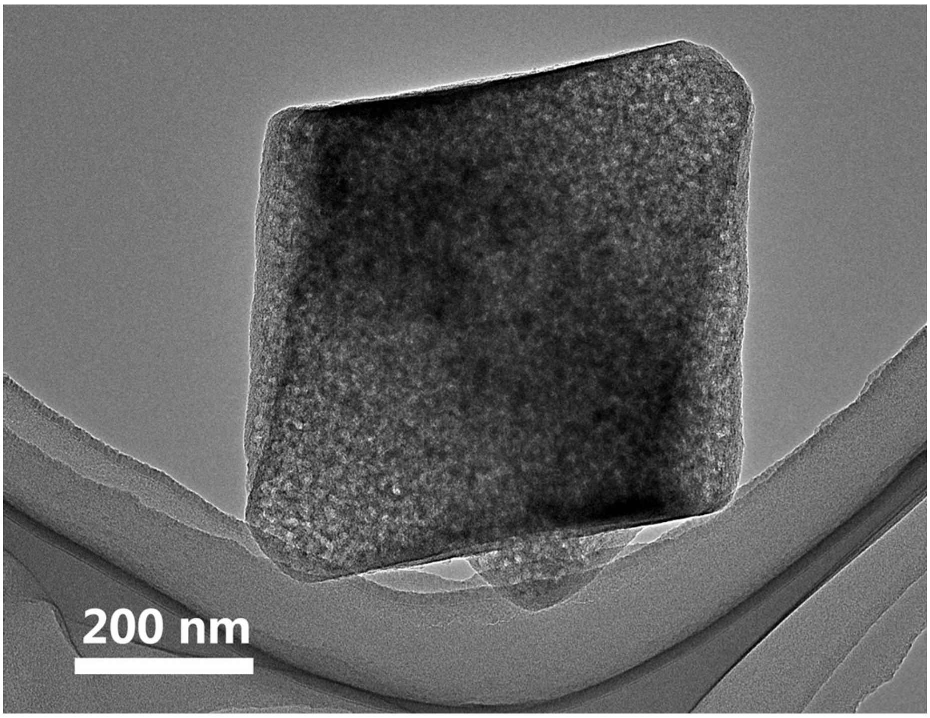

Figure S6. HRTEM of the as-made MoO_2@C nano-octahedron.

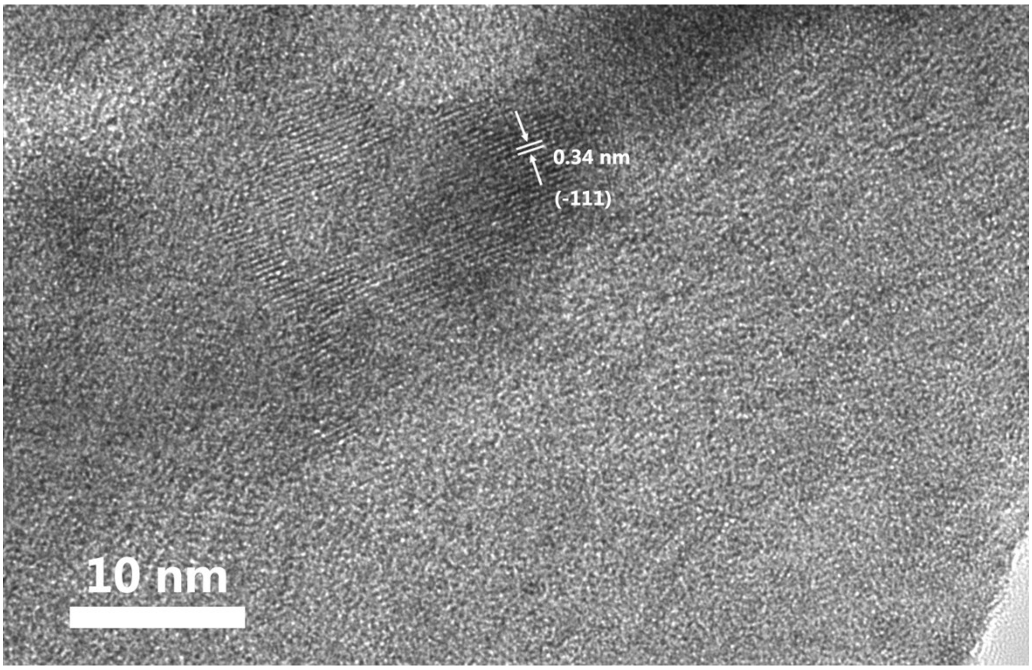

Figure S7. HRTEM of the as-made MoO_2@C nano-octahedron.

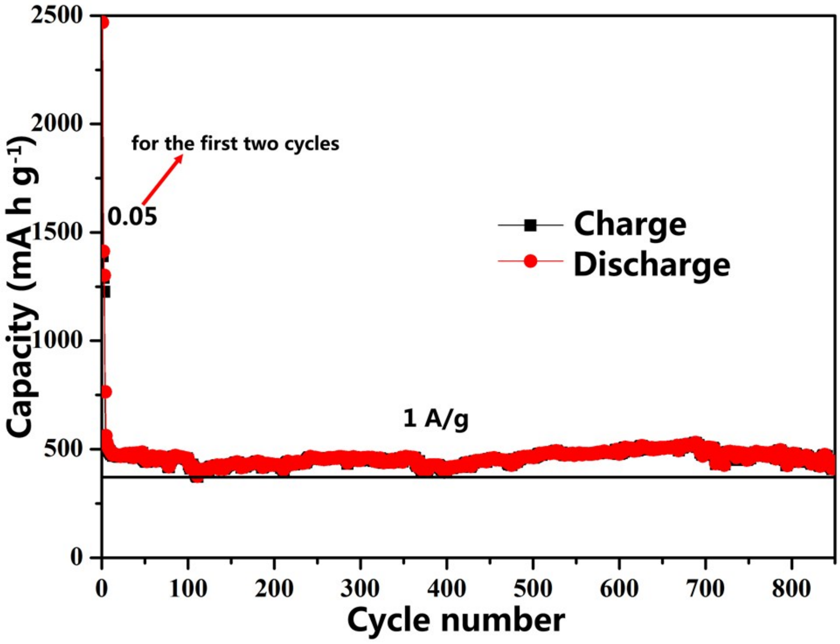

Figure S8. Cycling performance of MoO_2@C at a current density of 1 A g^{-1}.

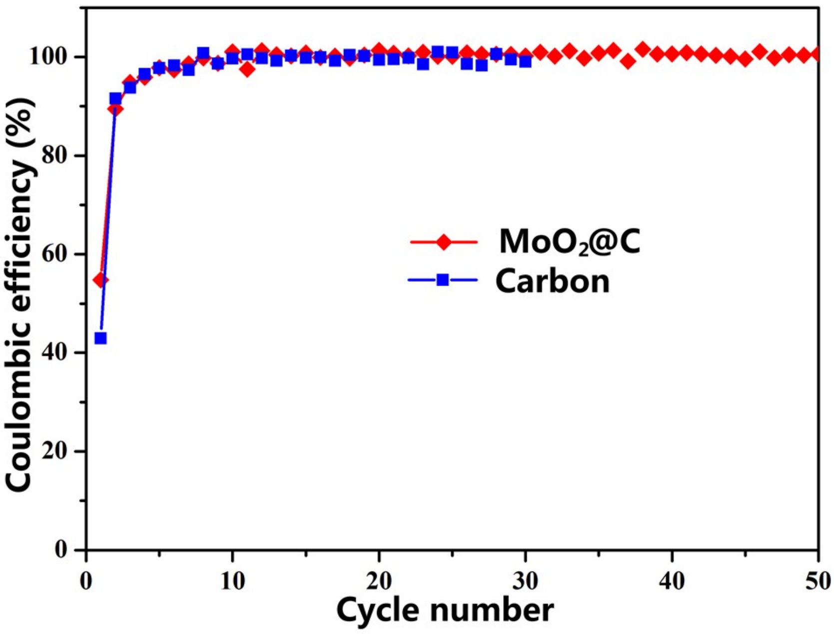

Figure S9. Coulombic efficiency of porous MoO_2@C nano-octahedrons and carbon matrix.

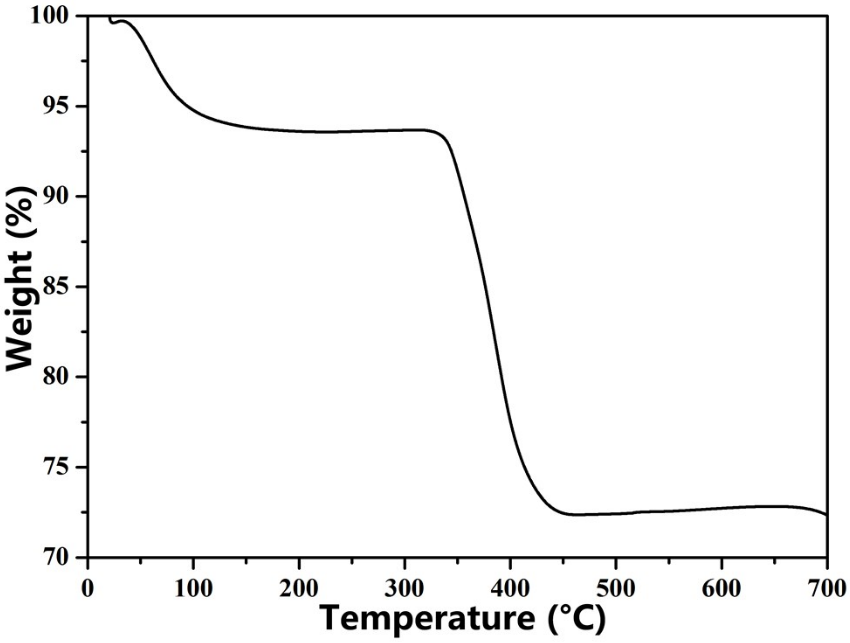

Figure S10.TGA curve of porous MoO_2@C nano-octahedrons in air.

The initial weight loss of 7% could be the weight of water, which were absorbed from the air. Then followed by the gradual oxidation of MoO_2 to MoO_3 and the combustion of carbon. Since the MoO_2 particles were homogeneous embedded in the carbon skeleton, the weight loss caused by the combustion of carbon could be the majority. Then a significant weight loss could happen. As the sample is composed of MoO_2 and carbon, and converts to only MoO_3 after heating to 600 °C with remaining weight of 72 wt.%. the MoO_2 content is estimated to be 68.8 wt% in the porous MoO_2@C nano-octahedrons according to the following equation: m (MoO_2) = 72 wt.% *M(MoO_2)/M(MoO_3)/(1-7 wt.%) = 72 wt.%*128/144/(93 wt.%) ≈ 68.8wt.%. And the carbon content is estimated to be 31.2 wt.%.

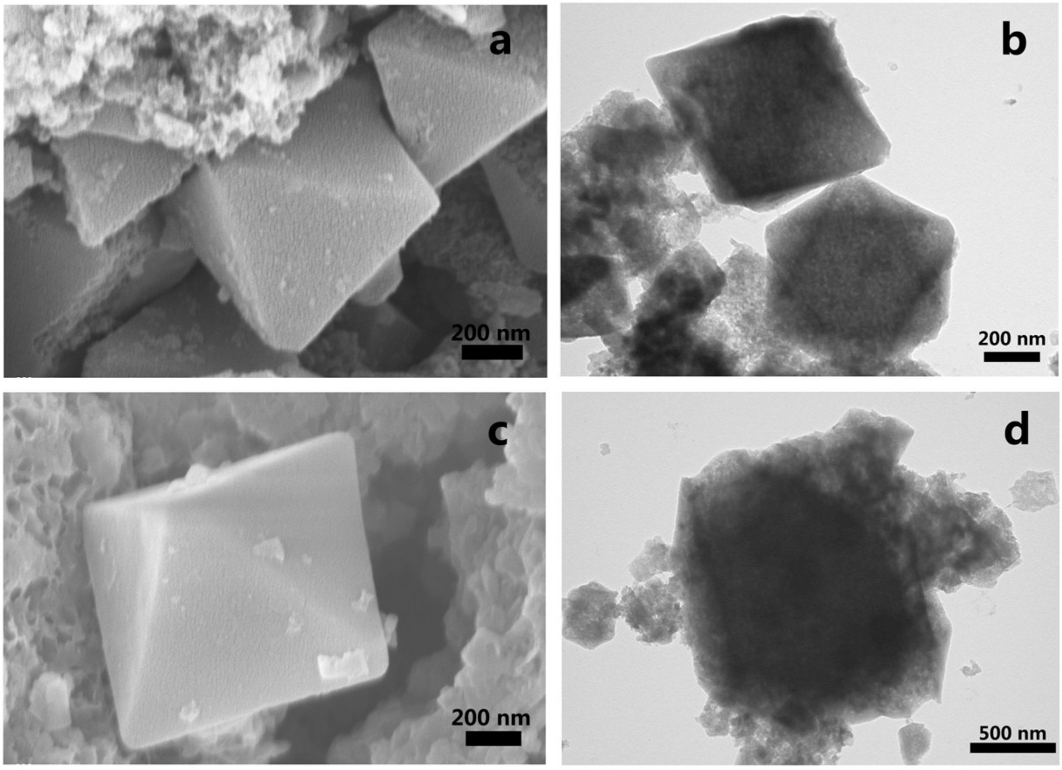

Figure S11. (a, b) SEM and TEM images of porous MoO_2@C nano-octahedrons after 50 cycles, (c, d) SEM and TEM of porous MoO2@C nano-octahedrons after 850 cycles.

Table S1. Comparison of BET specific surface area of various MoO2/C hybrid anode materials

Samples	BET specific surface area (m^2 g^{-1})	Reference
Porous MoO2@C nano-octahedrons	485	This work
MoO_2-ordered mesoporous carbon hybrids	304	1
Cage-like MoO_2-carbon	70.01	4
MoO_2-ordered mesoporous carbon	407	5
Carbon-coated MoO_2 nanospheres	31	7
Interconnected MoO_2 nanocrystals with carbon nanocasting	84.9	8
MoO_2-carbon nanowires	93.3	9
Carbon coated MoO_2 nanobelts	46.9	10
Hierarchical MoO_2-graphene	39.2	11
Graphene oxide-wrapped MoO2 porous nanobelts	44.89	15

Table S2. The comparison of the capacity of present work with reported MoO_2/C hybrid materials

Samples	Methods	Current density(mA g^{-1})	Cycle number	Capacity (mA h g^{-1})	Ref.
Porous MoO2@C nano-octahedrons	Solution and annealed	100	50	1442	This work
		1000	850	443.8	
MoO_2-ordered mesoporous carbon hybrids	Solvothermal	100	50	1049.1	1
MoO_2 nanoparticles embedded in carbon nanofibers	Solution and annealed	50	350	734	2
Hierarchical carbon-MoO_2 core-shell spheres	Hydrothermal	167.6	60	600	3
Cage-like MoO_2-carbon	Hydrothermal	200	80	692.5	4
MoO_2-ordered mesoporous carbon	Carbon thermal reduction	50	50	689	5
Hierarchical MoO_2-C spheres	Hydrothermal	200	150	812	6
Carbon-coated MoO_2 nanospheres	Hydrothermal and annealing	838	30	650	7
Interconnected MoO_2 nanocrystals with carbon nanocasting	Hydrothermal	200	70	640	8
MoO_2-carbon nanowires	Oil bath and calcination	200	20	500	9
Carbon coated MoO_2 nanobelts	Hydrothermal and calcination	100	30	617.2	10
Hierarchical MoO_2-graphene	Solution and anealed	1000	70	600	11
MoO_2-graphene thin film	Layer-by-layer self-assembly	47.8	100	675.9	12
3D graphene supported MoO_2	Chemical vaper deposition	200	150	986.9	13
MoO_2-graphene	Hydrothermal and calcination	100	60	1009.9	14
Graphene oxide-wrapped MoO2 porous nanobelts	Solution and hydrothermal	60	-	974	15

1. A. Chen, C. Li, R. Tang, L. Yin and Y. Qi, *Physical Chemistry Chemical Physics*, 2013, **15**, 13601-13610.
2. Y. Sun, X. Hu, W. Luo and Y. Huang, *Journal of Materials Chemistry*, 2012, **22**, 425-431.
3. J. Besnardiere, X. Petrissans, C. Surcin, V. Buissette, T. Le Mercier, M. Morcrette, D. Portehault and S. Cassaignon, *RSC Advances*, 2014, **4**, 21208-21215.
4. B. Liu, X. Zhao, Y. Tian, D. Zhao, C. Hu and M. Cao, *Physical Chemistry Chemical Physics*, 2013, **15**, 8831-8837.
5. L. Zeng, C. Zheng, C. Deng, X. Ding and M. Wei, *ACS Applied Materials & Interfaces*, 2013, **5**, 2182-2187.
6. H.-J. Zhang, T.-H. Wu, K.-X. Wang, X.-Y. Wu, X.-T. Chen, Y.-M. Jiang, X. Wei and J.-S. Chen, *Journal of Materials Chemistry A*, 2013, **1**, 12038-12043.
7. Z. Wang, J. S. Chen, T. Zhu, S. Madhavi and X. W. Lou, *Chemical Communications*, 2010, **46**, 6906-6908.
8. L. Zhou, H. B. Wu, Z. Wang and X. W. Lou, *ACS Applied Materials & Interfaces*, 2011, **3**, 4853-4857.
9. Q. Gao, L. Yang, X. Lu, J. Mao, Y. Zhang, Y. Wu and Y. Tang, *Journal of Materials Chemistry*, 2010, **20**, 2807-2812.
10. L. Yang, L. Liu, Y. Zhu, X. Wang and Y. Wu, *Journal of Materials Chemistry*, 2012, **22**, 13148-13152.
11. Y. Sun, X. Hu, W. Luo and Y. Huang, *ACS Nano*, 2011, **5**, 7100-7107.
12. F. Xia, X. Hu, Y. Sun, W. Luo and Y. Huang, *Nanoscale*, 2012, **4**, 4707-4711.
13. Z. X. Huang, Y. Wang, Y. G. Zhu, Y. Shi, J. I. Wong and H. Y. Yang, *Nanoscale*, 2014, **6**, 9839-9845.
14. Q. Tang, Z. Shan, L. Wang and X. Qin, *Electrochimica Acta*, 2012, **79**, 148-153.
15. W. Tang, C. X. Peng, C. T. Nai, J. Su, Y. P. Liu, M. V. V. Reddy, M. Lin and K. P. Loh, *Small*, 2015, **11**, 2446-2453.